PROCEEDINGS OF SPIE

SPIEDigitalLibrary.org/conference-proceedings-of-spie

A three-photon microscope with adaptive optics for deep-tissue in vivo structural and functional brain imaging

Xiaodong Tao, Ju Lu, Tuwin Lam, Ramiro Rodriguez, Yi Zuo, et al.

Xiaodong Tao, Ju Lu, Tuwin Lam, Ramiro Rodriguez, Yi Zuo, Joel Kubby, "A three-photon microscope with adaptive optics for deep-tissue in vivo structural and functional brain imaging," Proc. SPIE 10051, Neural Imaging and Sensing, 100510R (8 February 2017); doi: 10.1117/12.2253922

SPIE.

Event: SPIE BiOS, 2017, San Francisco, California, United States

A three-photon microscope with adaptive optics for deep-tissue in vivo structural and functional brain imaging

Xiaodong Tao*[a,c], Ju Lu[b,c], Tuwin Lam[a], Ramiro Rodriguez[a], Yi Zuo[b], Joel Kubby[a]
[a]W.M.Keck Center for Adaptive Optical Microscopy, Jack Baskin School of Engineering, University of California, Santa Cruz, CA 95064, USA
[b]Department of Molecular, Cell and Developmental Biology, University of California, Santa Cruz, CA 95064, USA
[c]*These authors contributed equally to this work*

ABSTRACT

We developed a three-photon adaptive optics add-on to a commercial two-photon laser scanning microscope. We demonstrated its capability for structural and functional imaging of neurons labeled with genetically encoded red fluorescent proteins or calcium indicators deep in the living mouse brain with cellular and subcellular resolution.

Keywords: Active or adaptive optics, Nonlinear microscopy, Fluorescence microscopy

1. INTRODUCTION

Two-photon (2P) microscopy is the leading technique for *in vivo* optical imaging deep into biological samples with subcellular resolution [1, 2]. However, its maximum imaging depth is limited to a few hundred micrometers due to scattering and refractive aberration in the tissue [3]. In order to increase the imaging depth, one can reduce scattering and absorption by selecting long excitation wavelengths in optical windows with low tissue absorption [4, 5]. One can also use adaptive optics (AO) to correct refractive aberration that increases the focal volume and hence decreases two-photon fluorescence emission [6-11]. Three-photon (3P) excitation enables imaging of fluorescent proteins (e.g., td-Tomato) and molecular sensors (e.g., red calcium indicators) at approximately 3 times the wavelength of their one-photon excitation peaks [12]. The third-order nonlinearity in 3P excitation also decreases the out-of-focus background light compared to 2P excitation [12, 13]. In this study we combine 3P excitation with AO, and demonstrate the capability of structural and functional imaging of neurons at the cellular and subcellular level in the living mouse brain.

2. METHOD

2.1 System setup

We integrated a 3P-AO add-on system (Fig. 1) into a commercial 2P laser scanning microscope (FV1000MPE, Olympus), so as to take advantage of its user-friendly hardware and software interfaces. The setup retains the option to feed the original tunable Ti:Sapphire laser (Mai Tai DeepSee, Spectra-Physics) for 2P imaging into our AO add-on system through a dichroic mirror (D1, Di02-R1064, Semrock), which provides the ability to conduct simultaneous multiple-excitation multiphoton imaging.

We used a fiber laser-based chirped pulse amplification system (FLCPA) (Cazadero, Calmar) as the 3P excitation light source. The FLCPA delivers up to 900 mW average power at 1550 nm; its repetition rate is tunable from 0.1 MHz to 25 MHz. Although the 1550 nm laser can generate 3P excitation for several fluorescent proteins, thermal damage due to water absorption in the living tissue limits imaging depth and duration. To minimize water absorption, we coupled the laser from the FLCPA into a photonic crystal rod (PCR, NKT Photonics) through the lens L1 (30 mm focal length, Thorlabs) to shift the output wavelength to around 1700 nm by soliton self-frequency shift [12]. Increasing the pulse energy shifts PCR output to longer wavelengths. The PCR confers the additional benefit of pulse compression [12]. The output beam from the PCR is collimated by the lens L2 (100 mm focal length, Thorlabs). The beam intensity can be adjusted with a variable metallic neutral density filter (NDC-50C-2, Thorlabs) installed on a computer-controlled servo. A long-pass filter with cut-on wavelength of 1580 nm (BLP01-1550R-25, Semrock) was used to block the residual pump laser. Second harmonic generation (SHG) and three-photon (3P) fluorescence are detected by channels 2 and 4 of the

Neural Imaging and Sensing, edited by Qingming Luo, Jun Ding, Proc. of SPIE Vol. 10051, 100510R · © 2017 SPIE · CCC code: 1605-7422/17/$18 · doi: 10.1117/12.2253922

microscope, respectively. The dichroic mirror with a 570nm cutoff wavelength in the Olympus filter cube (FV10-MRVGR/XRAC) can separate the emission signals between SHG and mCherry or RCaMP.

To optimize the wavelength for 3P imaging, we adjusted the pulse energy and the dispersion compensation to maximize signal intensity from fluorescent microspheres with regular water (H_2O) as the immersion medium. We measured the spectrum of the PCR output beam with an optical spectrum analyzer (Agilent 86146B), and the pulse width with a custom-built interferometric autocorrelator (not shown) using a similar design as described in [14]. The setup is based on a Michelson interferometer, where a reference mirror is installed on a nano-stage to scan the pulse separation. A Si detector (818-SL, Newport) in front of an objective lens is used as the nonlinear element to generate second harmonic at the output. A data acquisition card (PCIe-6363, National Instruments) is used to recorded the signal and generate the autocorrelation trace. The FLCPA repetition rate is set to 2 MHz, which provides 131 fs pulses, in close agreement with the manufacture's specification (126 fs pulse width). The pulse width is compressed to 80 fs by the PCR. After the objective lens the pulse is broadened to 99 fs due to dispersion in the optical system. We also measured the resolution of the microscope with fluorescent microspheres (diameter = 0.02 μm). The lateral and axial resolution is around 0.8 μm and 3 μm, respectively.

We implemented a sensorless AO scheme in the add-on system. We used a low-order continuous membrane deformable mirror (DM69, ALPAO) as the wavefront corrector. Its 69 actuators with 40 μm stroke can correct most of the low-order refractive aberrations in biological samples. Lenses L3 and L4 resize the incident beam to fit on the deformable mirror (DM). Lenses L5 and L6 conjugate the DM to the scanner in the FV1000MPV microscope frame. Inside the frame, a custom-made dichroic mirror (D2, not shown in Fig. 1) with a cutoff wavelength of 690 nm (Chroma) separates the excitation and emission light. Due to the high polarization dependence of dichroic mirrors, a half-wave plate is installed before the AO system to maximize the excitation power reflected by the dichroic mirror D2. The scanner and the tube lenses of the original Olympus microscope were replaced by lenses with a coating that is optimal around 1700 nm to increase the transmittance of the system. The excitation beam is fed into a 25x water-immersion objective with coating for high transmittance (~75%) around 1600 nm (XLPLN25XWMP2, NA 1.05, Olympus). Overall, the transmittance of the AO add-on is >80%, and the total transmittance of the microscope frame including the objective is around 60%.

The Olympus microscope and the AO add-on system are controlled by two computers. One computer is dedicated to operate the Olympus microscope control and image capturing software (FV10-ASW, Olympus). The other computer is equipped with a data acquisition card (PCIe-6363, National Instruments) to control the AO add-on system. The two computers are connected through an Ethernet cable. A custom software program written in Microsoft Visual C++ 2013 controls the AO system and synchronizes it with the FV1000MPE microscope using trigger signals from the latter.

2.2 System operation

Our 3P-AO add-on uses a simple modal sensorless wavefront correction scheme based on the Zernike modes, similar to the 3N algorithm [15]. In this scheme, phase aberration is represented as a linear combination of Zernike polynomials. Optimization proceeds in two steps: selection of a region-of-interest (ROI), and iterative wavefront correction (Fig. 2). In the ROI selection step, the scanned image is retrieved from the FV10-ASW software (microscope control) into the AO add-on software through the Ethernet connection, and a ROI on the image is selected by the user. A quality metric, defined as the cube root of the average signal intensity in the ROI, is computed. The signal can be either the fluorescence or the third harmonic generation (THG) channel of the image. THG signals can yield more stable results due to the absence of photobleaching. In the wavefront correction step, repeated for every sample, each Zernike mode is corrected sequentially. To increase the stability over a large aberration range, 5N method is applied in the system [15]. For each Zernike mode, five images are taken with the phases displayed on the DM defined as $(k_i + j\varphi)Z_i$, where i indexes the Zernike mode, k_i is the index factor of the mode, φ is the search step size, and j indexes the steps from -2 to 2. The quality metrics on the five images are computed and fit with a Gaussian function [15]. Then the phase corresponding to the peak of the quality metric is calculated. Optimization proceeds through all the modes up to order M = 22. Since defocus is coupled with the spherical aberration, additional defocus is applied to compensate for the focal plane shift during the optimization of spherical aberration. Depending on the amplitude of the aberrations, multiple iterations of optimization may be applied. The optimization time is limited by the microscope's image acquisition software and the file transfer between the two computers. It takes 20 seconds for one iteration. Bypassing the Olympus software could further improve the operation speed. After the final phase is set on the DM, 3P imaging can be performed using the microscope PC. For imaging of a small volume, such as shown in Fig. 8 (118μm × 118μm × 63μm), a single correction is applied for the whole image stack. The corrected volume depends on the isoplanatic patch for specific samples [16]. For larger volume imaging, multiple corrections may be required to achieve a wider correction volume.

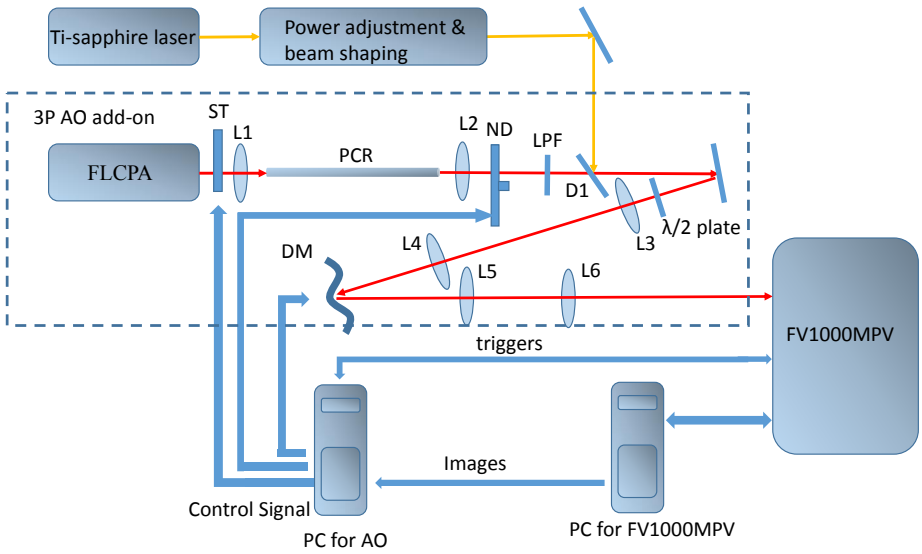

Figure 1. (a) System diagram. L, lens; DM, deformable mirror; ST, shutter; ND, variable metallic neutral density filter; LPF, long pass filter; D1, dichroic mirror; PCR, photonic crystal rod.

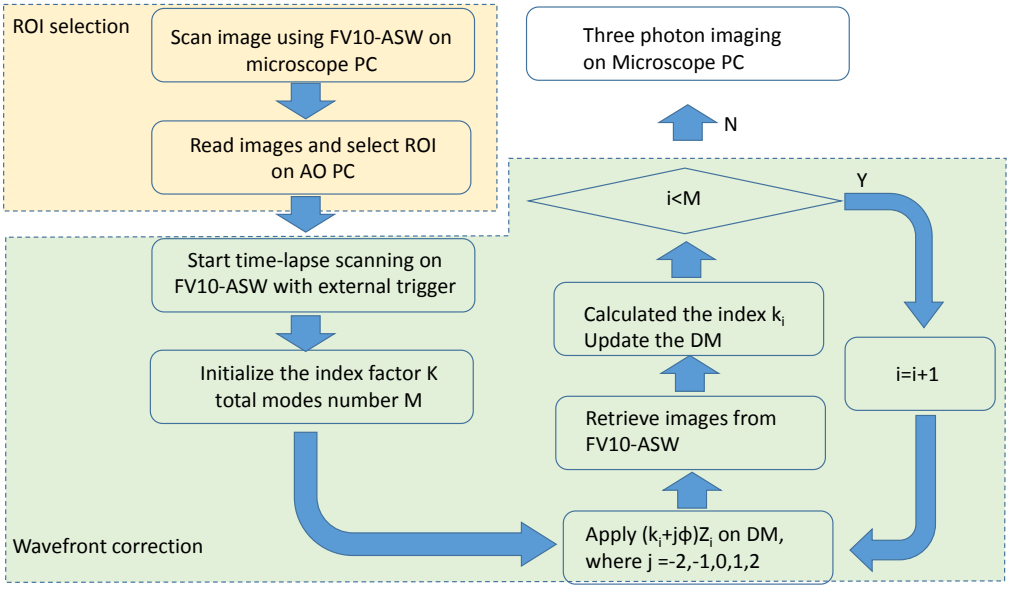

Figure 2. Flow chart for sensorless wavefront correction

2.3 Sample preparation

Fluorescent microspheres with 0.02 µm diameter (Invitrogen, 580/605) were used to measure microscope resolution. Fluorescent microspheres with 1.1 µm diameter (Invitrogen, 540/560) were used to test wavefront correction. The microspheres were spread onto a glass slide with mounting medium (Fluoromount-G, Cell Lab) and sealed with a 170 µm cover slip.

We used several transgenic mouse lines in conjunction with viral injection to label selected populations of neurons with either structural markers (red fluorescent proteins) or functional sensors (red calcium indicators). A cross between Gad2-IRES-Cre (JAX #010802) and Ai14(RCL-tdT)-D (JAX #007908) mouse line was used to label inhibitory interneurons with cytosolic td-Tomato. The Thy1-GFP line M mice (JAX #007788) received intracortical injection of adeno-associated viruses (AAV) encoding the Cre-DOG system and Flex-td-Tomato (both generously provided by Dr. Constance L. Cepko and Dr. Jonathan C. Y. Tang at Harvard Medical School) to sparsely label deep layer neurons and their dendritic structures with td-Tomato. The C57BL/6J mice received intracortical injection of AAV encoding the Cre recombinase and floxed jRGECO1a for calcium imaging (both purchased from University of Pennsylvania Vector Core). Mice 6 weeks or older of both sexes were used in this study. All procedures were conducted in accordance with protocols approved by the Institutional Animal Care and Use Committee, University of California Santa Cruz.

The mouse was anesthetized with isoflurane (1.5%) and injected with dexamethasone (2mg/kg body weight) intramuscularly and carprofen (0.3 ml from 0.50 mg/ml stock) intraperitoneally to prevent brain swelling. The craniotomy was performed with a trephine (Fine Science Tools) driven by a high-speed micro drill (Foredom). A chronic imaging glass window was then implanted and secured with cyanoacrylic glue (Vetbond). A custom head-plate was secured onto the skull with dental acrylic. At the end of surgery, buprenorphine (0.1 mg/kg body weight) and enrofloxacin (5 mg/kg body weight) were injected subcutaneously to reduce pain and prevent infection, respectively. For structural imaging of neurons and dendrites, mice were anesthetized by intraperitoneal injection of a mixture of ketamine (87 mg/kg body weight) and xylazine (8.7 mg/kg body weight).

3. Experimental results

3.1 3P-AO imaging of fluorescent microspheres

With 3P excitation, fluorescence emission scales as the cube of excitation intensity. To verify the order of nonlinearity in our system, we measured fluorescence intensity of microspheres under different excitation power (Fig. 3). We fit the data with both quadratic and cubic curves, and found that the cubic curve fit better. In addition, the same excitation power generated much stronger fluorescence emission when heavy water (D_2O) was used instead of regular water (H_2O) as the immersion medium, because D_2O absorbs much less at this wavelength than H_2O [12].

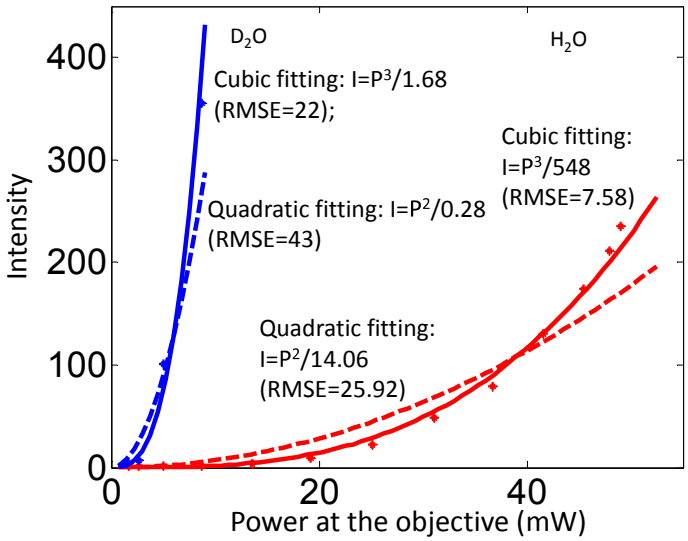

Figure 3. Cubic scaling relationship between fluorescence emission and excitation power at the objective indicates three-photon excitation. Cubic and quadratic curve fitting are shown as solid and dashed curves, respectively. RMSE, root mean square errors.

Refractive aberrations affect 3P imaging more severely than 1P or 2P imaging due to the higher order non-linearity[10]. In order to characterize the aberration-induced signal loss, we used the DM to introduce primary spherical aberrations with different amplitudes, and measured the intensity of fluorescence emitted by microspheres. We found a cubic decay with the root mean square (RMS) of the wavefront (Fig. 4a). To test the correction ability of the AO system, we then introduced spherical aberration by adjusting the correction collar on the objective lens and corrected it with the DM. The RMS wavefront error due to the collar adjustment was around 0.15λ, which reduced the signal intensity (Fig. 4b, left panel). The RMS wavefront error is estimated by the final shape of the pre-calibrated DM after optimization. If this error is fully corrected by AO, the signal intensity should be improved by more than two-fold as predicted by the scaling relationship shown in Fig. 4(a). Indeed, AO correction restored the wavefront (Fig. 4d) and markedly improved the signal to noise ratio as expected (Fig. 4b-c).

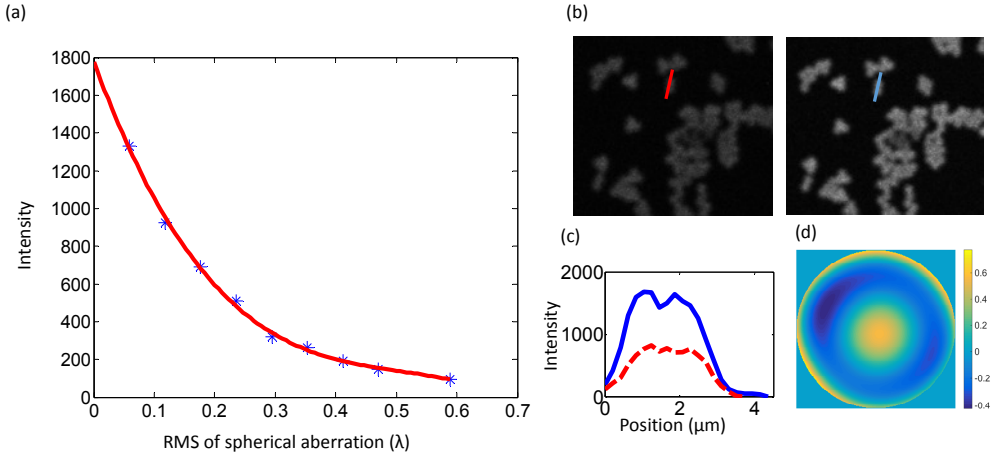

Figure 4. 3P-AO imaging of fluorescent microspheres. (a) Fluorescence intensity decreases as spherical aberration increases. Red line: cubic curve fitting. (b) Images of microspheres before and after AO correction, where the aberration was introduced by adjusting the correction collar of the objective lens. (c) The intensity profiles along the lines in (b). (d) The final phase on the DM.

3.2 3P imaging of the live mouse brain

We then tested the ability of the add-on system for *in vivo* 3P imaging in the mouse brain. The laser power was increased gradually with the imaging depth from 5 mW to 90 mW. Figure 5(a) shows imaging of cortical neurons labeled with td-Tomato. The images were collected with a Z step size of 3 μm. The fluorescence signal in the td-Tomato channel remains fairly strong down to a depth of 750 μm. Imaging of the THG signal in the brain tissue, which likely includes contributions from lipid-rich structures such as myelin sheaths of axons and blood vessels [17], shows that the add-on system is able to penetrate up to 1 mm below dura mater (Fig. 5b). At a more moderate depth, the system can resolve dendritic spines (minuscule protrusions on neuronal dendrites, which host the postsynaptic sites of the majority of excitatory synapses) without AO correction, as shown in the maximum intensity projection image from 440 μm to 490 μm depth (Figure 5c). The spine head and the parent dendritic branch, separated by only 2.4 μm, are clearly resolved (Figure 5d).

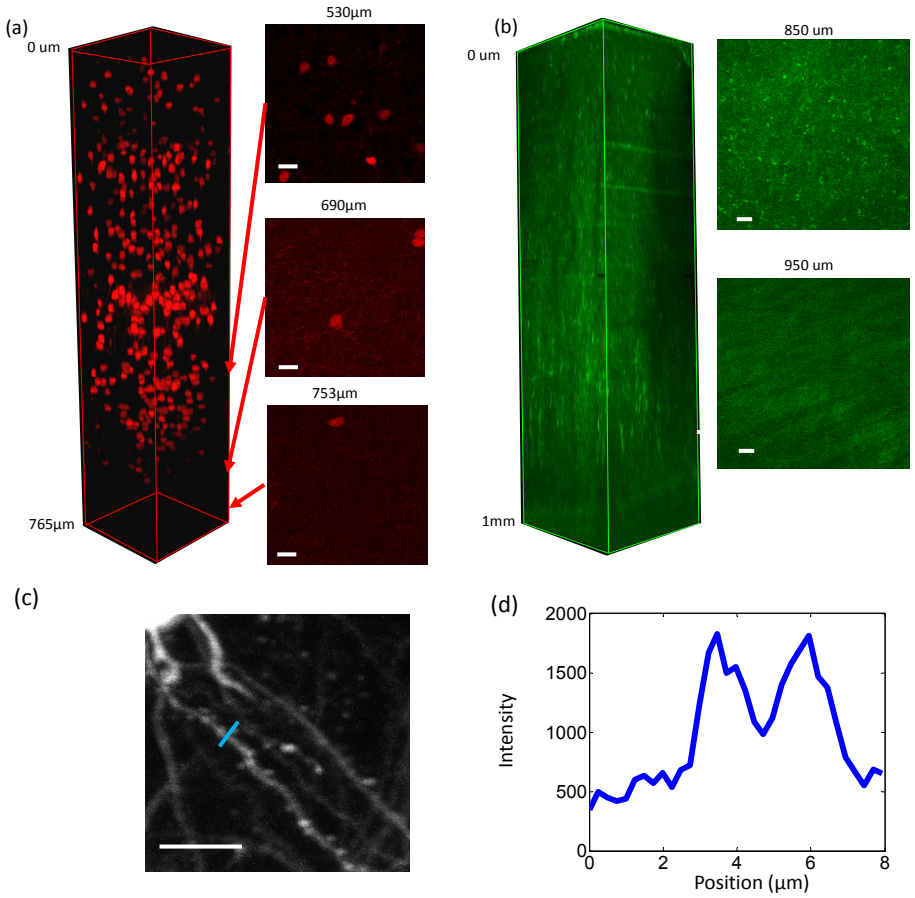

Figure 5. Three-photon imaging of the live mouse brain. (a) Imaging of neurons labeled with td-Tomato up to a depth of 765µm (Visualization 1 and 2). (b) Deep THG imaging up to a depth of 1mm (Visualization 3 and 4). (c) 3P imaging of dendritic spines from 440µm to 490µm below the cortical surface (Visualization 5). (d) Intensity profile along the line across the dentrite and the spine in (c). Scale bar, 20µm.

The long excitation wavelength of red-fluorescent calcium indicators facilitates deep brain imaging. Thus we tested the ability of our system for 3P imaging of the genetically encoded calcium indicator jRGECO1a. The mouse was placed on a custom-built rotating disk with its head secured to a metal holder via the head-plate. It remained awake throughout the experiment and could voluntarily run on the disk. Fig. 6(a) shows an example of jRGECO1a-labeled neurons in the motor cortex, and Fig. 6(b) shows calcium transients ($\Delta F/F_0$) of these neurons. This result shows the ability of 3P excitation of red fluorescent calcium indicators for functional imaging.

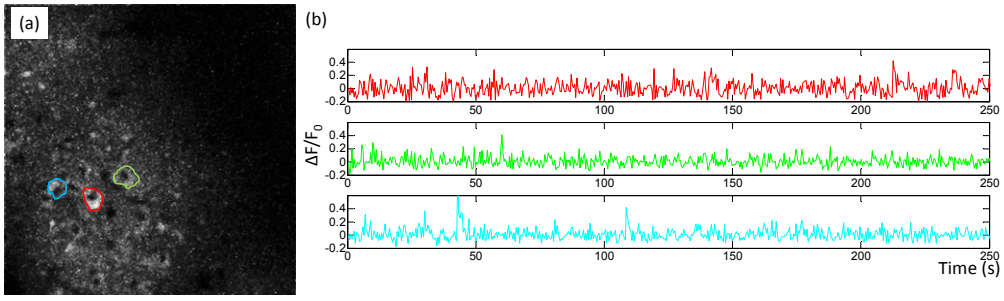

Figure 6. 3P calcium imaging of cortical neurons in awake mouse (Visualization 6 and 7). (a) Maximum intensity projection of the time series of neurons labeled with the genetically encoded red calcium indicator jRGECO1a. Images were taken with 256 x 256 pixels per frame at 2.33 Hz (pixel dwelling time = 2 µs). (b) Calcium transients of selected neurons in (a) shown as $\Delta F/F_0$.

3.3 3P imaging of live mouse brain with wavefront correction

We tested the effect of the AO add-on for *in vivo* deep brain imaging by applying wavefront correction at the depth from 505 µm to 543 µm below the cortical surface. The strong signal from the td-Tomato-labeled cell bodies provided a good reference for sensorless wavefront correction. A 10x10 µm ROI was selected over a cell body as shown in Fig. 7(a). The DM was optimized by maximizing the average intensity in the ROI. The RMS wavefront error before correction was found to be around 0.18λ. Figure 7(b) shows the image after correction. Applying the final phase (Fig. 8d) on the DM significantly improves signal intensity across the entire 250x250 µm field of view (compare Fig. 7a with 7b). The intensity profiles along the lines across two dendrites show more than three-fold improvement.

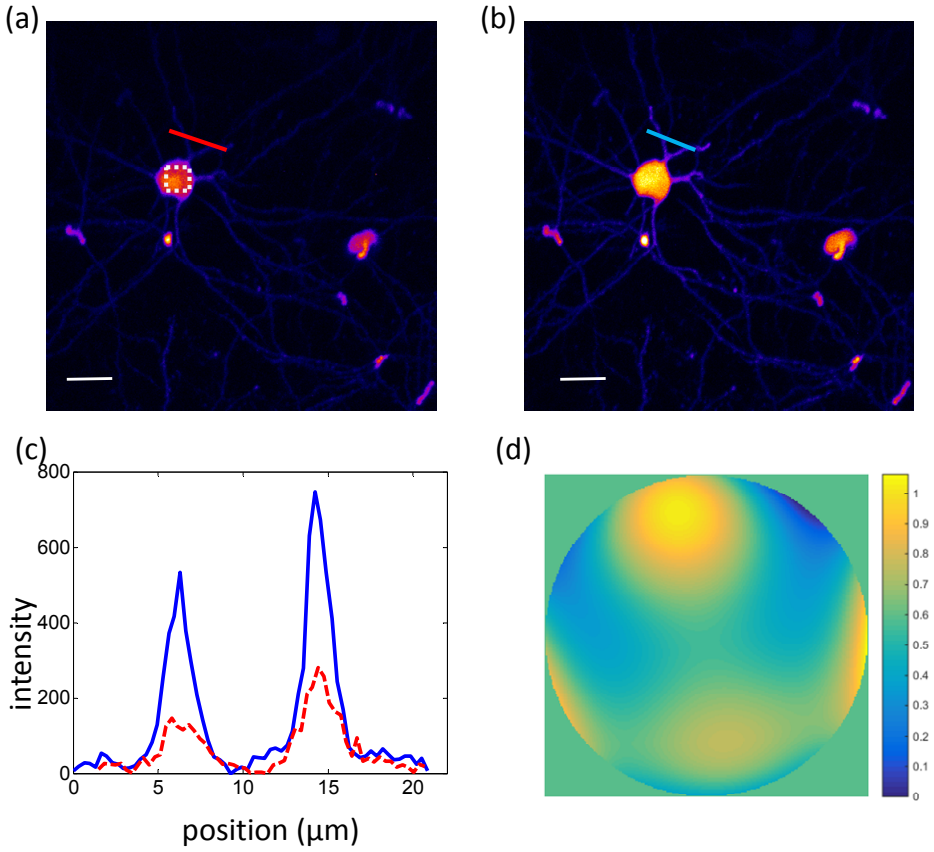

Figure 7. 3P-AO imaging of neurons in a live mouse brain (Visualization 8). (a,b) Neurons at the depth from 505 µm to 543 µm below the cortical surface (a) without and (b) with AO correction. Dashed square: ROI selected as reference. (c) Intensity profiles along the lines in (a,b). (d) The final phase on the DM, RMS = 0.18λ

Conclusion and Discussion

In conclusion, we have developed a 3P-AO add-on system on a commercial laser scanning microscope that is equipped with a Ti:Sapphire laser for 2P imaging up to 1060 nm. We added a 1550 nm femtosecond fiber laser chirped pulse amplification system and a photonic bandgap crystal that shifts the wavelength up to 1700 nm for 3P microscopy. The

maximum average power and the pulse width after the objective lens of the microscope were measured to be ~100 mW and ~100 fs, respectively. Using this system we have demonstrated 3P structural imaging of td-Tomato labeled neuronal somata, dendrites and dendritic spines in live mouse brains, and showed that AO improved fluorescence intensity by over three-fold at the depth of 505 μm to 540 μm below the cortical surface. We have also demonstrated functional imaging of cortical neurons labeled with the genetically encoded red calcium indicator jRGECO1a in awake, head-restrained mice. Overall, we have demonstrated the feasibility of *in vivo* structural and functional imaging in the mouse brain with our add-on system, which will help disseminate the use of 3P and AO for biological imaging.

Acknowledgements

This material is based upon work supported by the National Science Foundation under Grant Number 1429810. Any opinions, findings, and conclusions or recommendations expressed in this material are those of the authors and do not necessarily reflect the views of the National Science Foundation. The multiphoton microscope that was modified was provided by the California Institute for Regenerative Medicine (CIRM) Shared Stem Cell Facility under Grant Number CL1-00506-1.1. The results presented herein were obtained at the W.M. Keck Center for Adaptive Optical Microscopy (CfAOM) at University of California Santa Cruz. The CfAOM was made possible by the generous financial support of the W.M. Keck Foundation. This material is also based upon work supported by the UC Office of the President for the UC Work Group for Adaptive Optics in Biological Imaging, by the Multicampus Research Programs and Initiatives (MRPI), Grant #MR- 15-327968. Dr. Ju Lu was supported by the California Blueprint for Research to Advance Innovations in Neuroscience (Cal-BRAIN) program award for "Three-Photon Microscopy with Adaptive Optics for Deep Tissue Brain Activity Imaging." We would like to thank Dr. Constance L. Cepko and Dr. Jonathan C. Y. Tang for providing CRE-DOG and Flex-td-Tomato vectors; Dr. Chia-Chien Chen for providing the Gad2-IRES-Cre x Ai14(RCL-tdT)-D mice; Dr. Benjamin Abrams (UCSC Life Sciences Microscopy Center) for technical support; Marc R. Reinig, Dr. Qinggele Li, and Samuel W. Novak for helpful discussions.

REFERENCES

[1] Helmchen, F. and Denk, W., "Deep tissue two-photon microscopy," Nat. Methods 2, 932-940 (2005).
[2] Svoboda, K. and Yasuda, R., "Principles of two-photon excitation microscopy and its applications to neuroscience," Neuron 50, 823-839 (2006).
[3] Theer, P., Hasan, M. T. and Denk, W., "Two-photon imaging to a depth of 1000 mu m in living brains by use of a Ti : Al2O3 regenerative amplifier," Opt. Lett. 28, 1022-1024 (2003).
[4] Kobat, D., Durst, M. E., Nishimura, N., Wong, A. W., Schaffer, C. B. and Xu, C., "Deep tissue multiphoton microscopy using longer wavelength excitation," Opt. Express 17, 13354-13364 (2009).
[5] Shi, L. Y., Sordillo, L. A., Rodriguez-Contreras, A. and Alfano, R., "Transmission in near-infrared optical windows for deep brain imaging," J. Biophotonics 9, 38-43 (2016).
[6] Debarre, D., Botcherby, E. J., Watanabe, T., Srinivas, S., Booth, M. J. and Wilson, T., "Image-based adaptive optics for two-photon microscopy," Opt. Lett. 34, 2495-2497 (2009).
[7] Ji, N., Milkie, D. E. and Betzig, E., "Adaptive optics via pupil segmentation for high-resolution imaging in biological tissues," Nat. Methods 7, 141-147 (2010).
[8] Tang, J. Y., Germain, R. N. and Cui, M., "Superpenetration optical microscopy by iterative multiphoton adaptive compensation technique," Proc. Natl. Acad. Sci. U.S.A. 109, 8434-8439 (2012).
[9] Tao, X. D., Norton, A., Kissel, M., Azucena, O. and Kubby, J., "Adaptive optical two-photon microscopy using autofluorescent guide stars," Opt. Lett. 38, 5075-5078 (2013).
[10] Sinefeld, D., Paudel, H. P., Ouzounov, D. G., Bifano, T. G. and Xu, C., "Adaptive optics in multiphoton microscopy: comparison of two, three and four photon fluorescence," Opt. Express 23, 31472-31483 (2015).
[11] Wang, K., Sun, W. Z., Richie, C. T., Harvey, B. K., Betzig, E. and Ji, N., "Direct wavefront sensing for high-resolution in vivo imaging in scattering tissue," Nat. Commun. 6 (2015).

[12] Horton, N. G., Wang, K., Kobat, D., Clark, C. G., Wise, F. W., Schaffer, C. B. and Xu, C., "In vivo three-photon microscopy of subcortical structures within an intact mouse brain," Nat. Photonics 7, 205-209 (2013).
[13] Wang, K., Horton, N. G., Charan, K. and Xu, C., "Advanced Fiber Soliton Sources for Nonlinear Deep Tissue Imaging in Biophotonics," IEEE J. Sel. Top. Quantum Electron. 20 (2014).
[14] N. G. Horton and C. Xu, "Dispersion compensation in three-photon fluorescence microscopy at 1,700 nm," Biomed. Opt. Express **6**(4), 1392–1397 (2015).
[15] Facomprez, A., Beaurepaire, E. and Debarre, D., "Accuracy of correction in modal sensorless adaptive optics," Opt. Express 20, 2598-2612 (2012).
[16] O. Azucena, J. Crest, J. Cao, W. Sullivan, P. Kner, D. Gavel, D. Dillon, S. Olivier and J. Kubby, "Wavefront aberration measurements and corrections through thick tissue using fluorescent microsphere reference beacons," Optics Express **18**(16), pp. 17521-17532 (2010).
[17] S. Witte, A. Negrean, J. C. Lodder, C. P. J. de Kock, G. T. Silva, H. D. Mansvelder, and M. L. Groot, "Label-free live brain imaging and targeted patching with third-harmonic generation microscopy," Proc. Natl. Acad. Sci. U.S.A. 108, 5970-5975 (2011).